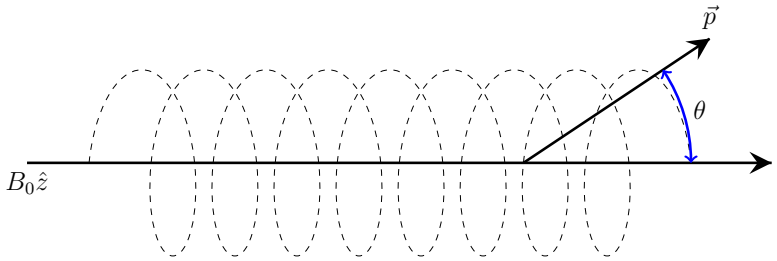

Figure 1 Motion of a particle through a magnetic field. Scattering with pitch angle θ

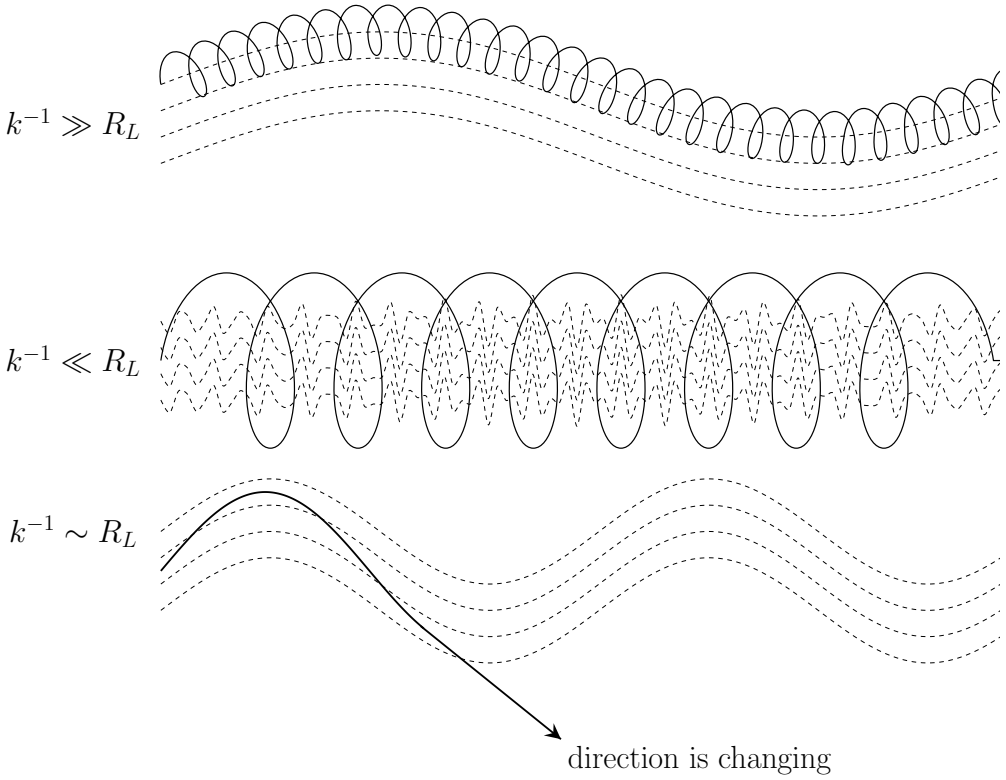

Figure 2 Particle trajectory (solid line) on the perturbed magnetic field (dashed line).

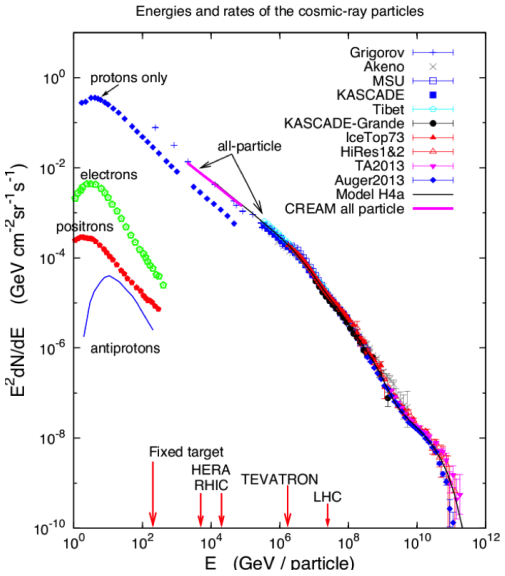

Figure 3 Cosmic ray spectrum as measured on earth by several experiments. Figure taken from [1].

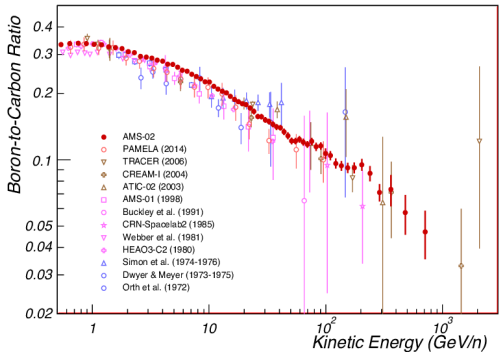

Figure 4 Boron to carbon ratio as a function of energy per nucleon as measured by several cosmic ray experiments. Figure taken from [2].

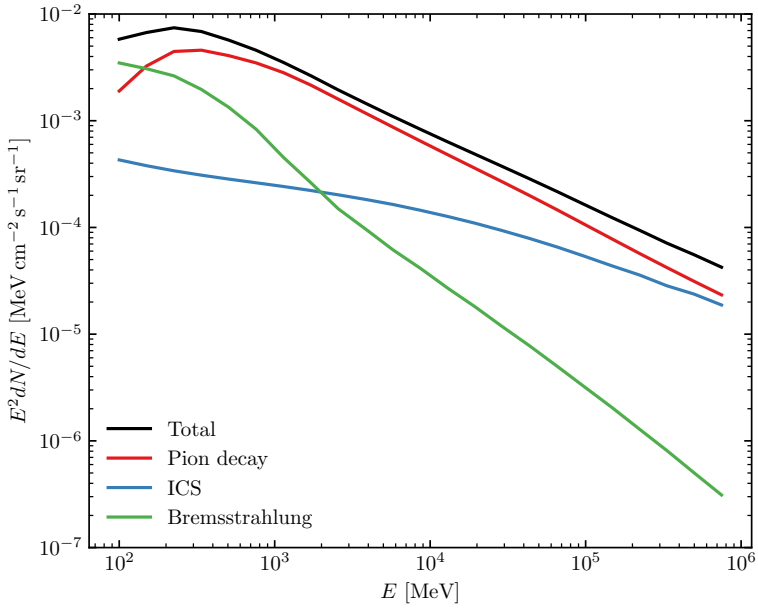

Figure 5 Spectra of the main components of diffuse gamma-ray emission according to a regular GALPROP-webrun.

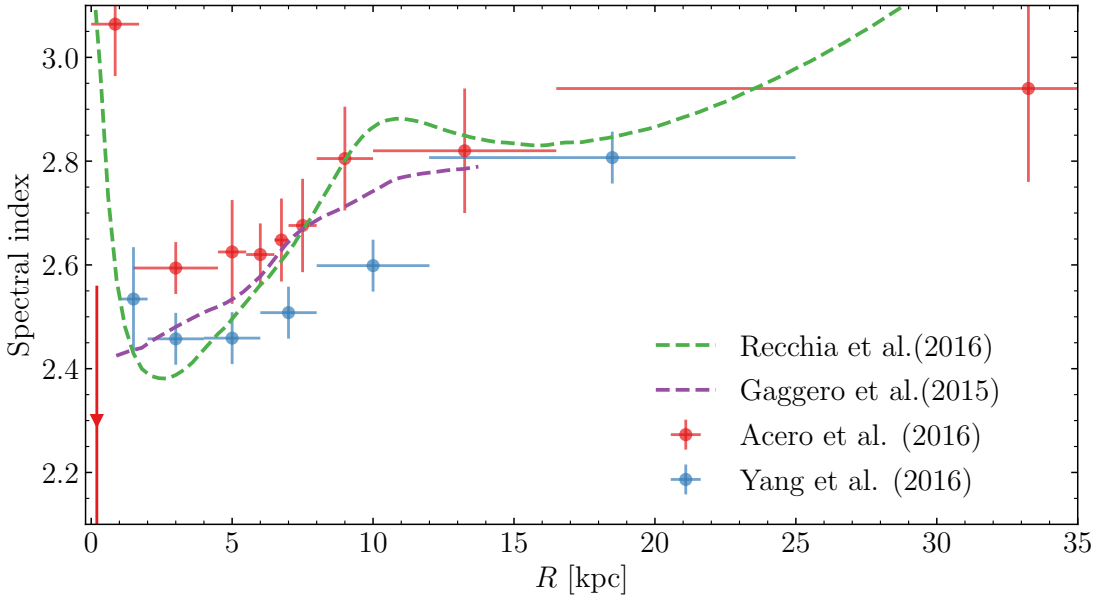

Figure 6 The spectral hardening as observed by [3, 4] with predictions by [5, 6]. The most inner point from [4] is the CMZ. Also note that [3] give the photon index above 2 GeV and [4] give the proton index P_2 from fitting a proton spectrum of the form $\beta^{P_1}\rho^{P_2}$, where $\beta = v/c$ and ρ is the rigidity.

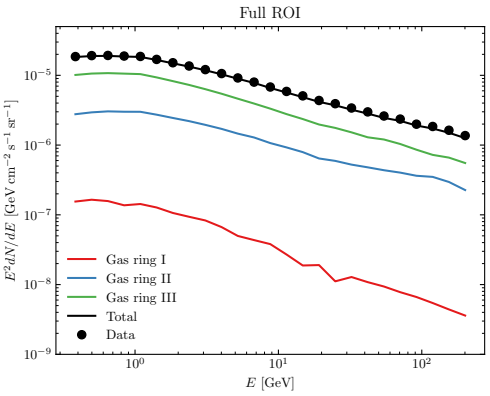

Figure 7 Spectra of the gas rings from `RUN5` [7]

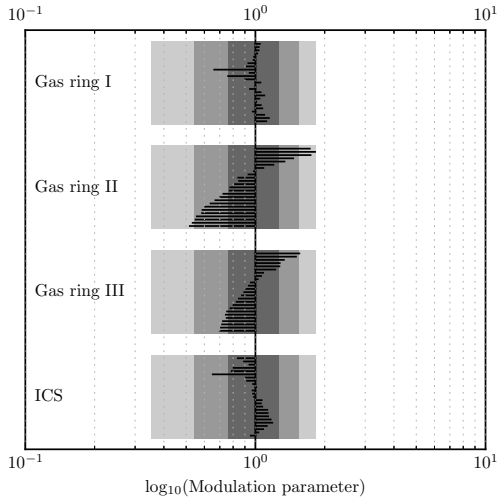

Figure 8 Rescaling of spectra from `RUN5` in [7]. See Figure 12 for a detailed description.

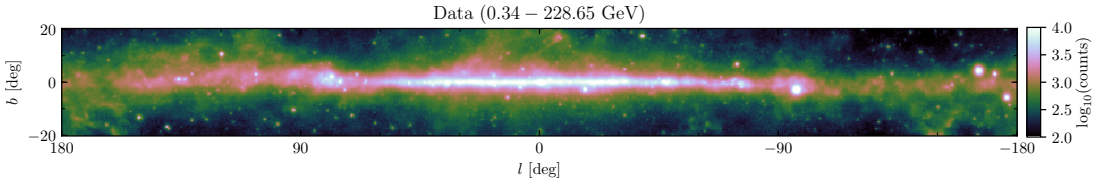

Figure 9 The pre-processed Fermi-LAT data used for this analysis.

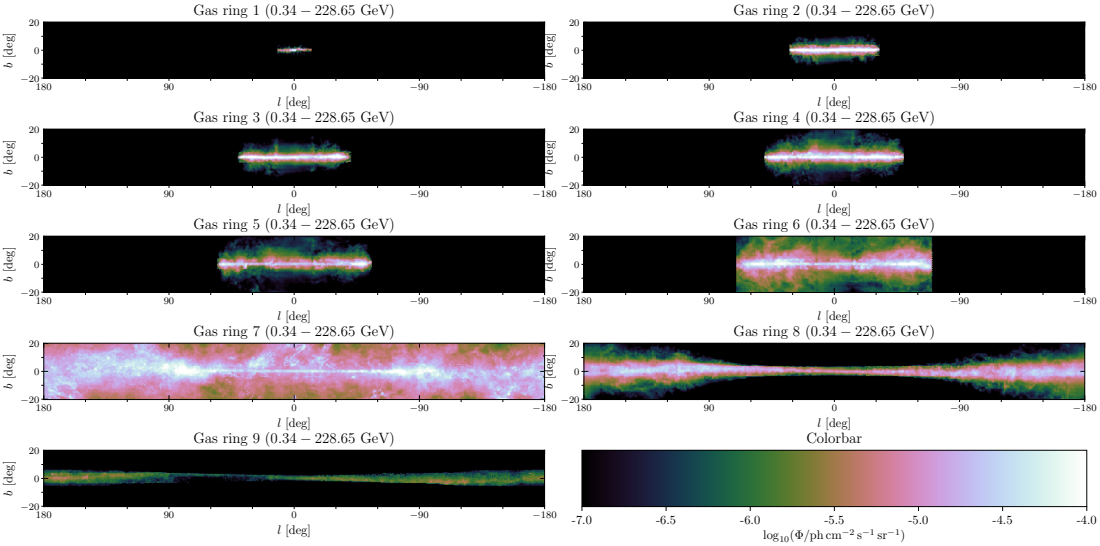

Figure 10 Templates of the gas maps, post-fit

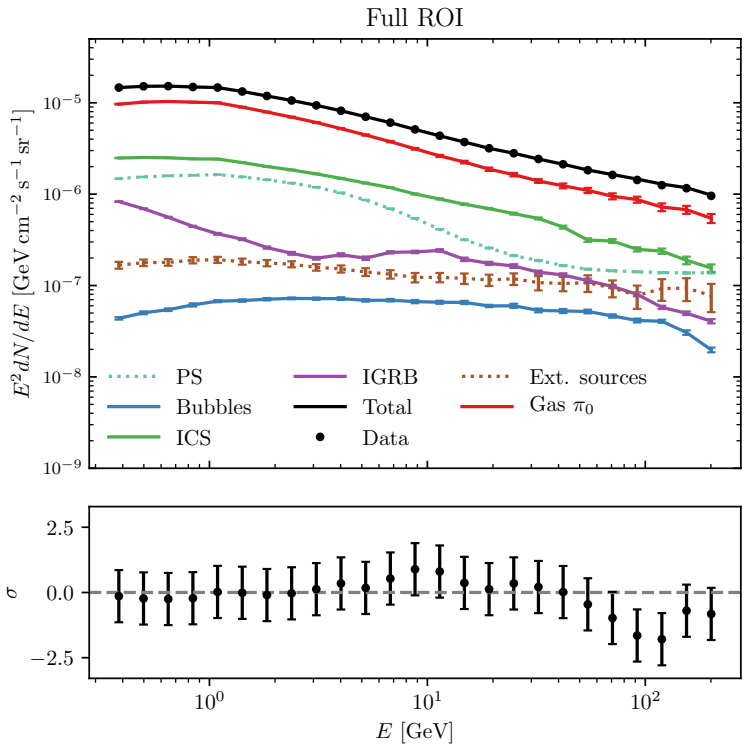

Figure 11 Spectra of the components over the whole region. Gas components are added together for clarity. The residuals are given in the bottom panel in units of standard deviation $\sigma = (\text{data} - \text{model})/\sqrt{\text{model}}$.

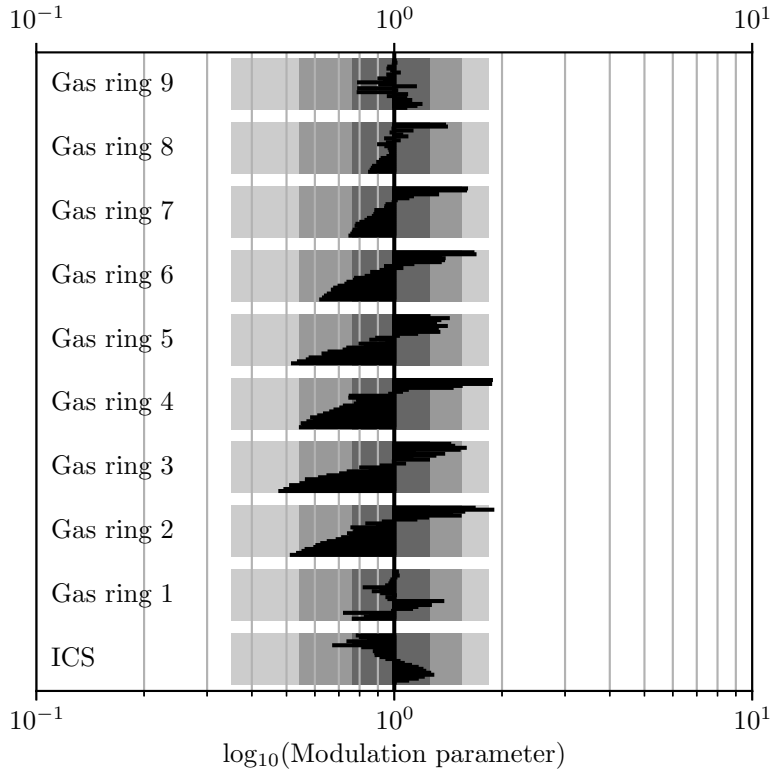

Figure 12 Spectral rescaling of the run as shown in **??**. The black lines correspond to the value of the spectral nuisance parameter σ in each energy bin (bottom to top: $0.3 - 230$ GeV). The differently shaded gray regions are the 1,2 and 3-σ ranges corresponding to the MEM regularization where $\lambda = 16$.

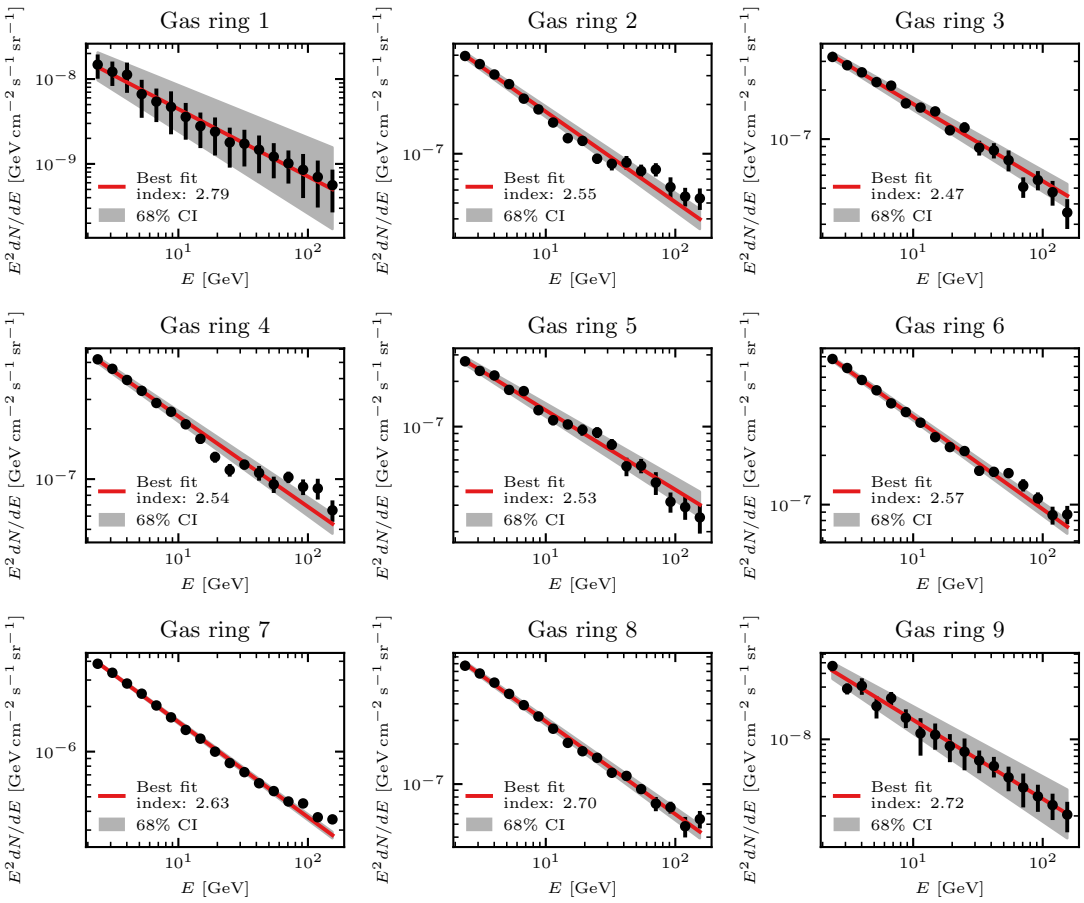

Figure 13 Spectrum of gamma-ray emission attributed to different gas rings 1-9 with the best fit power-law from $2 - 230$ GeV and the 68% credible interval.

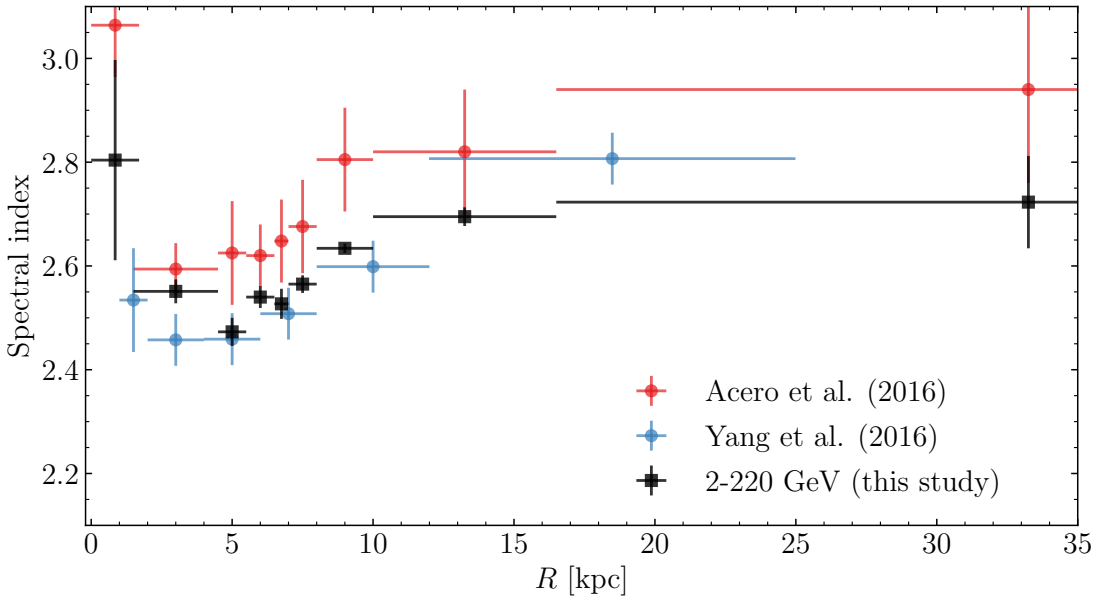

Figure 14 Spectral index of gamma rays associated with pion decay at different radii from the galactic center. Shown here the spectral index fitted as explained in the text from $2 - 230$ GeV compared to the trend found in [3, 4].

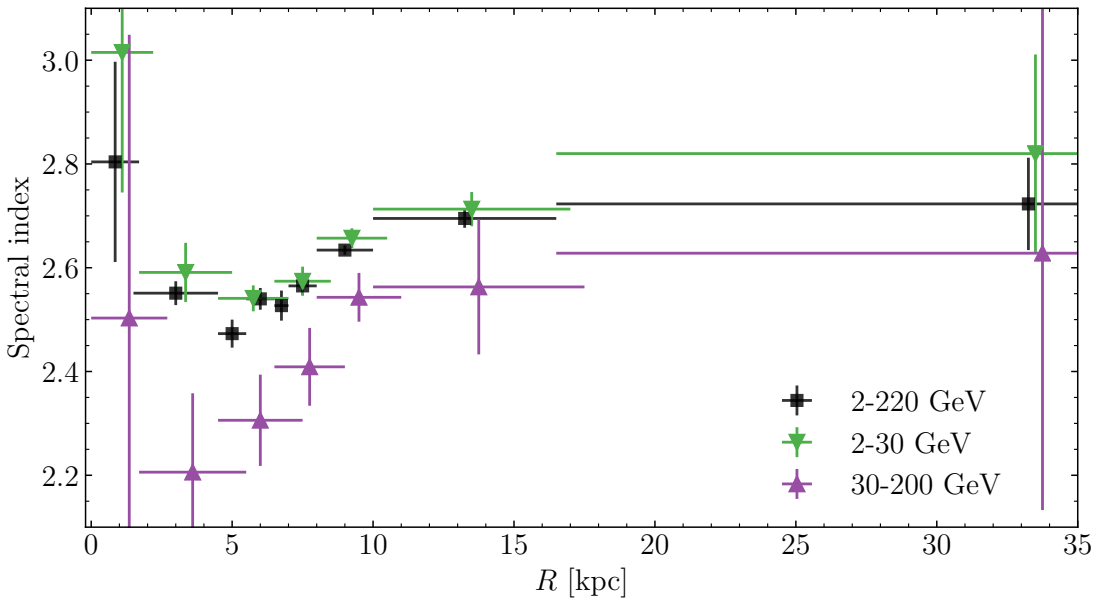

Figure 15 Spectral index of gamma rays associated with pion decay at different radii from the galactic center. The index from $2 - 30$ GeV and $30 - 220$ GeV are shifted to the right by 0.25 kpc and 0.5 kpc respectively so that the error-bars do not overlap. Error-bars are 68% credible intervals.

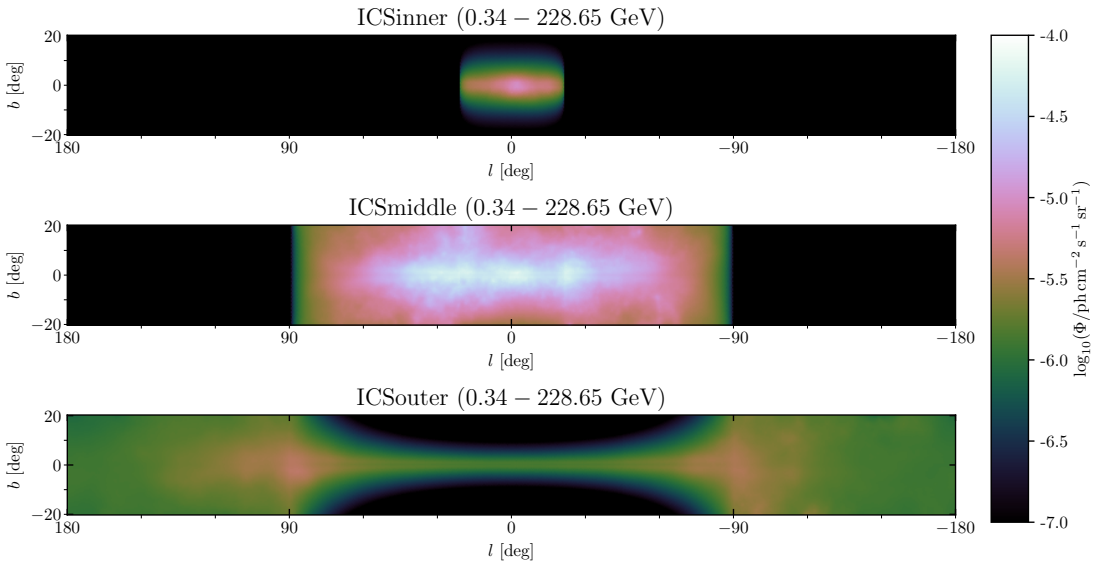

Figure 16 ICS template split over 3 rings. The three rings correspond to $0-3$,$3-8.3$ and $8.3-50$ kpc respectively from top to bottom.

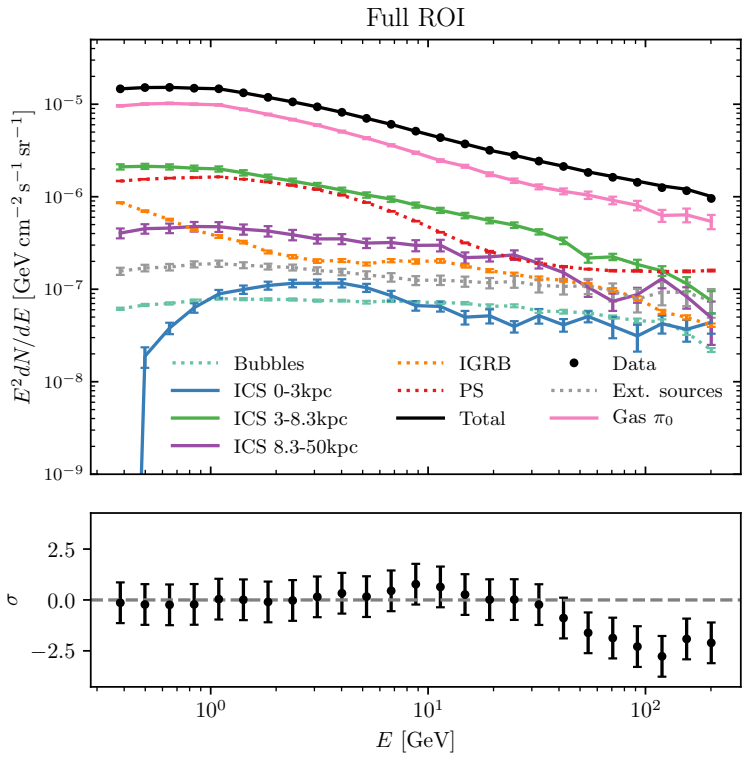

Figure 17 Spectra of all components in the fit with the ICS template split over three rings.

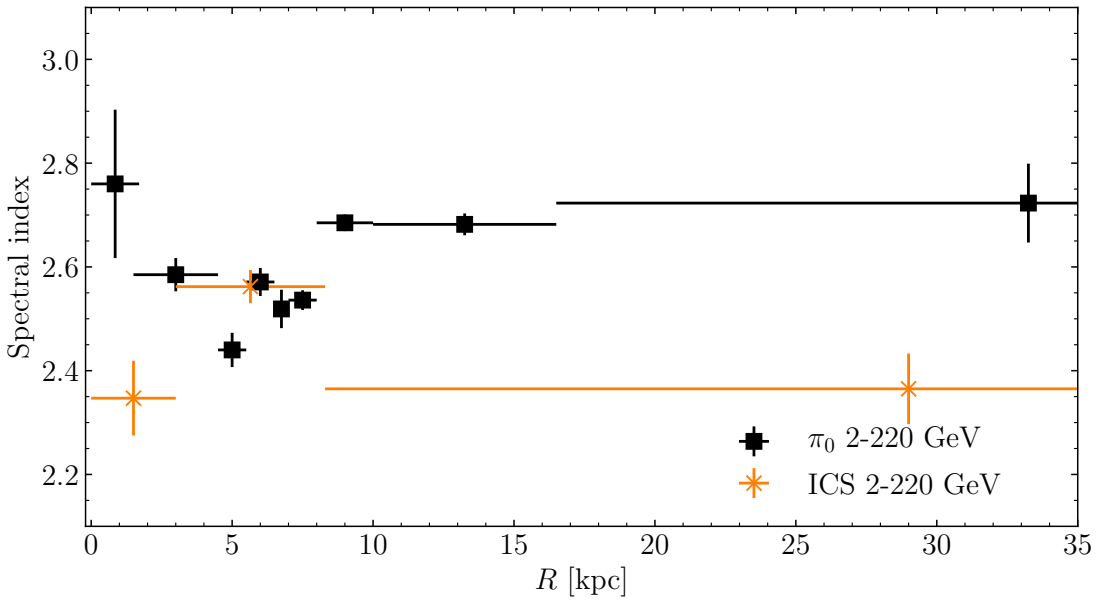

Figure 18 Spectral index for the run with the ICS template split over three rings.

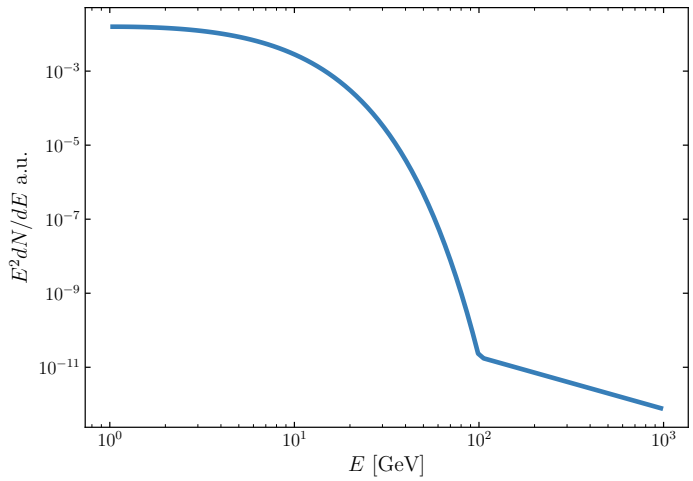

Figure 19 Log-average spectrum of 3FGL and 3FHL galactic sources

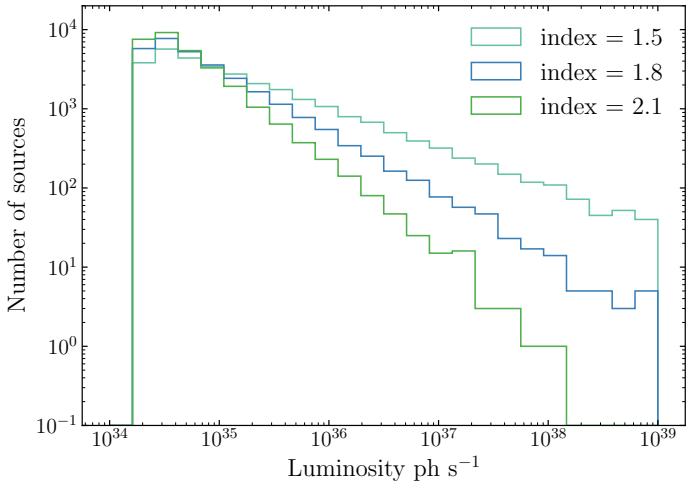

Figure 20 Histogram of luminosities with 3fgl source counts

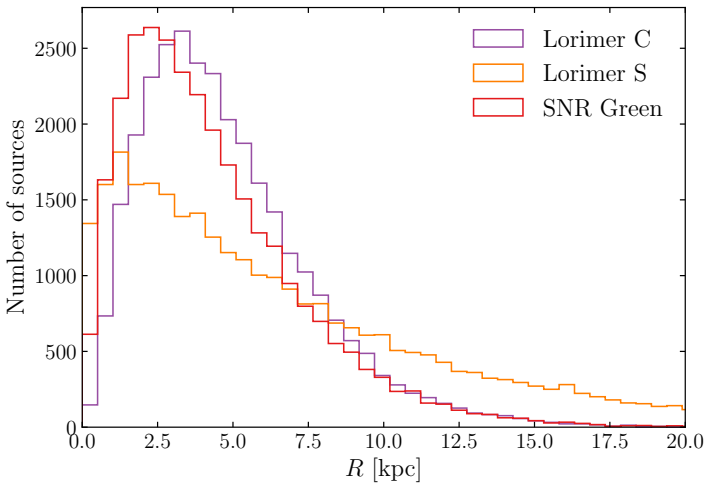

Figure 21 Histogram of radius of simulation with 30000 sources.

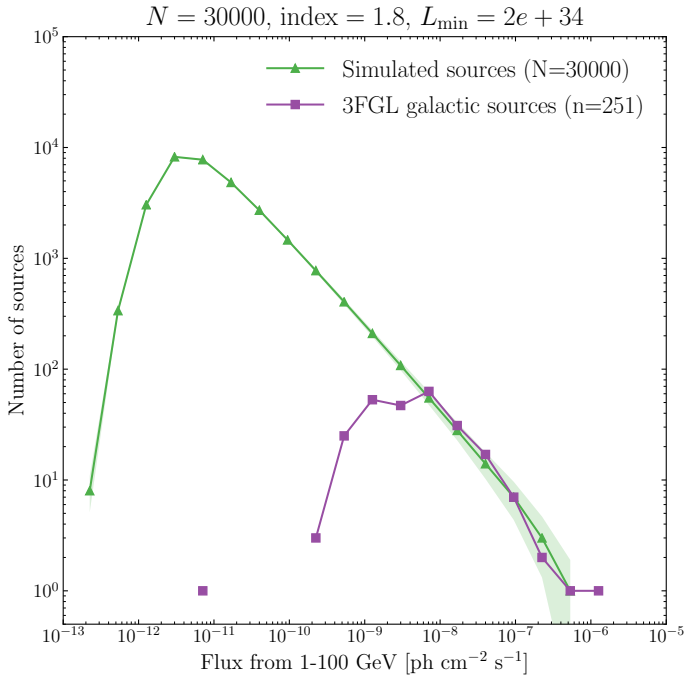

Figure 22 Dependence of source counts vs flux. All galactic 3fgl sources.

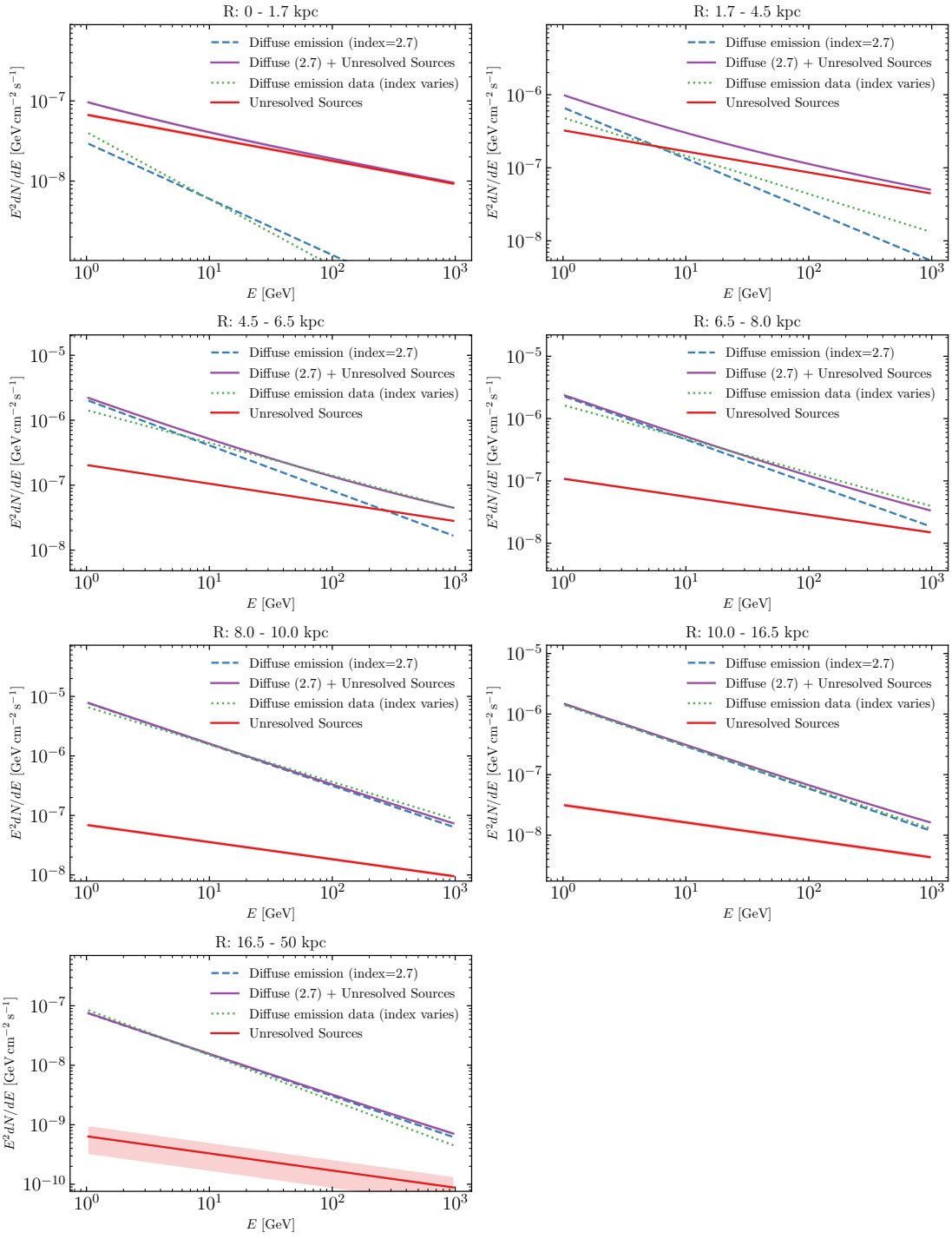

Figure 23 Spectra of unresolved sources with a hard powerlaw spectrum (2.2) and diffuse emission.

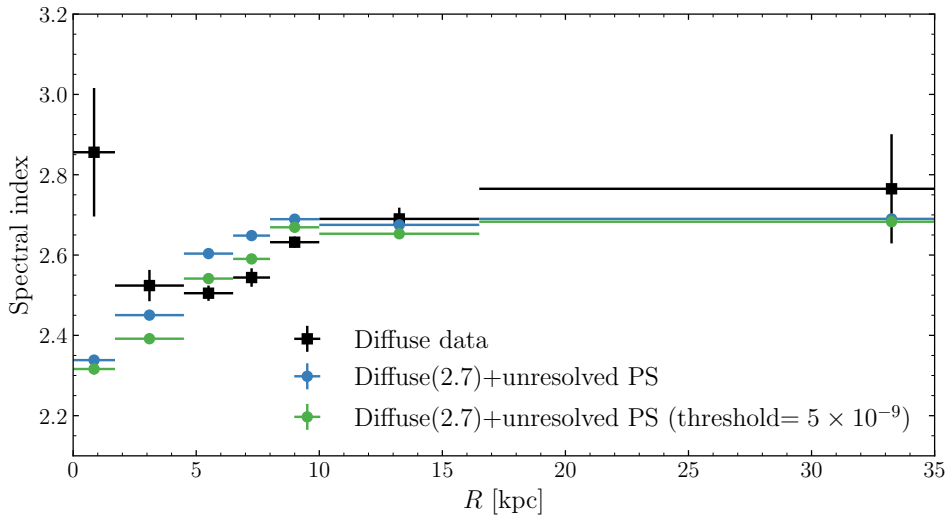

Figure 24 Spectral index of diffuse emission (assuming it is a powerlaw with index 2.7) plus the emission from unresolved sources (flux $< 5 \times 10^{-10}$ and flux$< 5 \times 10^{-9}$).

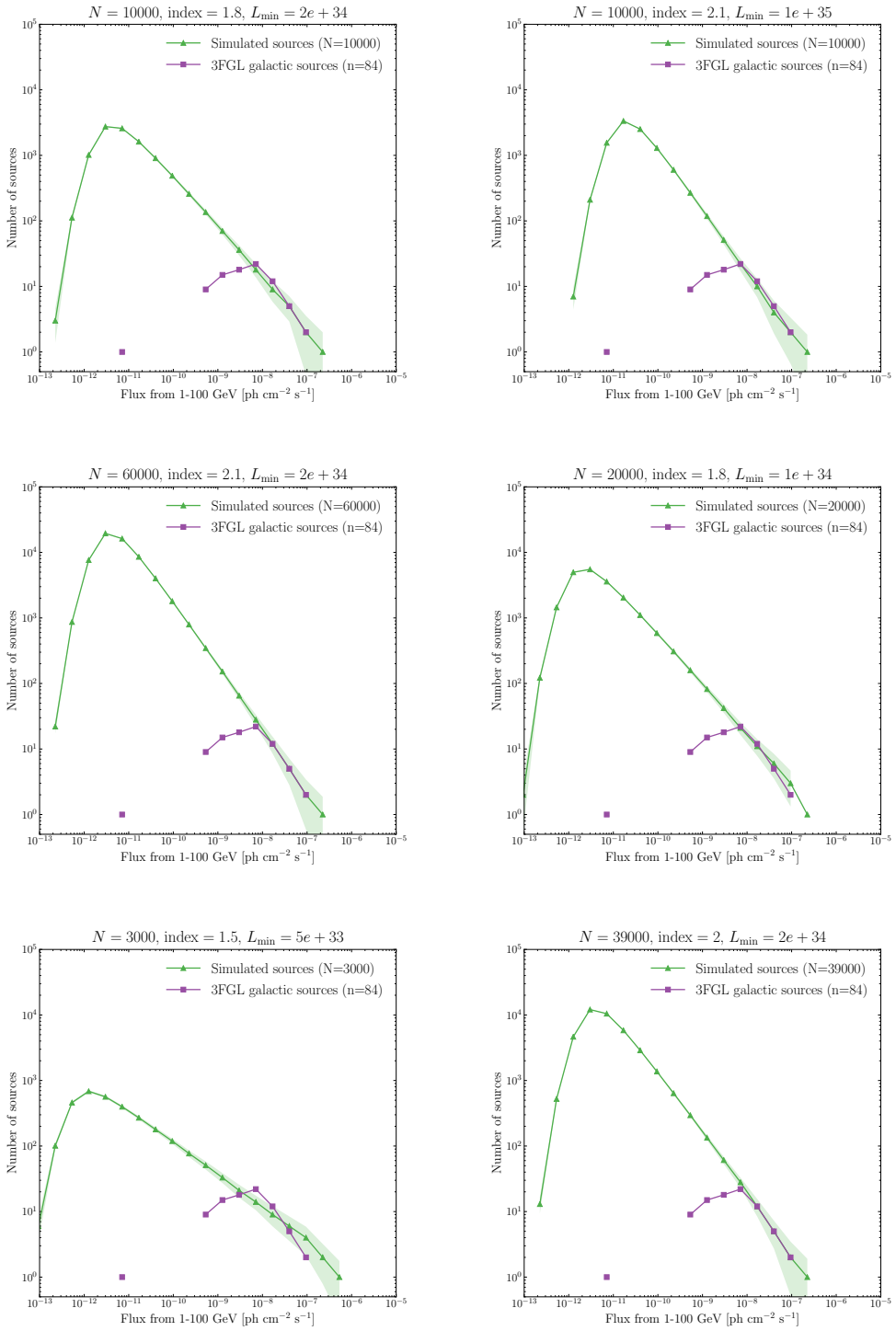

Figure 25 Histogram of flux vs source counts of different simulations.

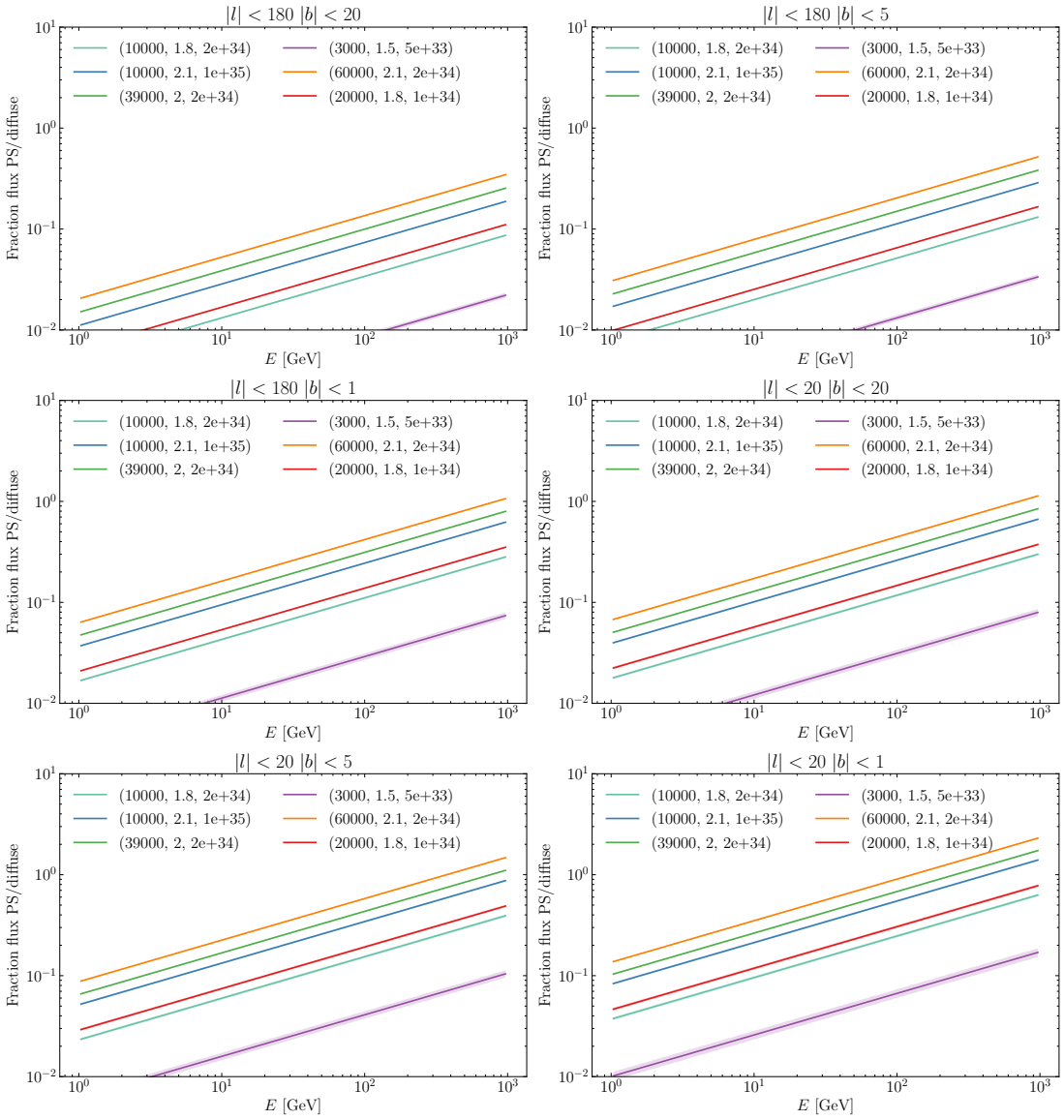

Figure 26 Fraction of PS/diffuse for simulations as in Figure 24 for several regions in the sky.

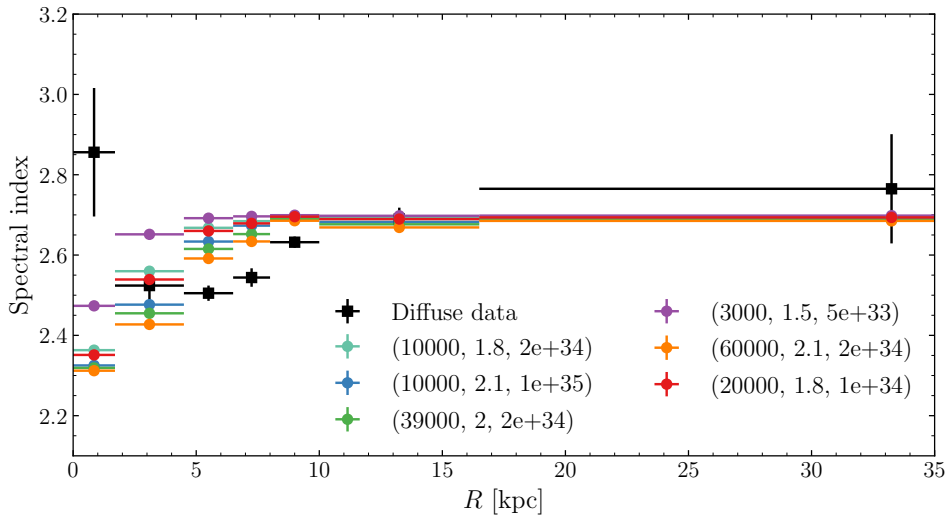

Figure 27 Spectral index for simulations as in Figure 24. The legend corresponds to: (Number of sources, luminosity function index, $L_{\min}$)